

Application of Contact Surface Model for Modelling Subject-specific Human Tibiofemoral Joint Motion

Jeffrey Hartanto¹, Wee Kheng Leow¹, Andy Khye Soon Yew², Joyce Suang Bee Koh², Tet-Sen Howe²

¹National University of Singapore, Singapore, SG, ²Singapore General Hospital, Singapore, SG

Email: jhartanto@comp.nus.edu.sg

INTRODUCTION: A computational model that can model subject-specific joint motion is crucial for routine clinical practice such as pre-operative planning. For routine clinical practice, the model should not require complex auxiliary data, such as motion capture data and multiple computed tomography (CT)/ magnetic resonance imaging (MRI) scans. [1] proposed a contact surface model (CFM) that can generate sufficiently accurate patellofemoral (PF) joint motion with one set of knee CT scans and a few landmarks placed on the bone. However, it is still unclear whether the CFM could be applied to generate motion of other joints without significantly reducing its accuracy. This paper evaluates the accuracy of the CFM to generate tibiofemoral (TF) joint motion. Thus, this study highlights the reliability of the CFM for modelling other joints' motion.

METHODS: CT scans of five cadaver knees (age: 53–78 years; 4 males and 1 female; 3 left and 2 right knees) were captured between 0° and 120° flexion angles at intervals of 30°. For each subject, the 3D models of the femur and the tibia were segmented and constructed from the CT scans. The models at 0° served as the input of the CFM, and the models at the other flexion angles served as the ground-truth data. As describe in [1], CFM consists of three stages: (1) model construction, (2) tibia pose estimation and (3) tibia motion generation. In (1), three landmarks called condyle landmarks (Fig. 1) are placed at the most protruding part of the medial condyle where the tibia rolls and glides. They are used to define in-plane translation and flexion of tibia pose with respect to the femur. The most proximal condyle landmark, or termination landmark, (Fig. 1) denotes the end position of the tibia with respect to the femur. To model tilting and internal/external rotation of the tibia, two refinement landmarks are placed on each side of tibia (Fig. 1). In (2), a motion plane, P , is constructed by fitting a plane to the condyle landmarks to locate intersection curves on the bone models. For an approximation of combined cartilage thickness, our model uses the distance of closest point, D , between the intersection curves of the bone models at 0° (Fig. 2). With three distinctive points that describe a tibia pose (Fig. 2), three motion paths are generated in the normal direction of femoral intersection curve that maintain constant gap D between the two bones, until they reach the termination landmark (Fig. 3). Next, P is centered at each refinement landmark to find their respective intersection curves. Then, two refinement paths that maintain their respective distances at 0° are generated, similar to motion path generation (Fig. 3). In (3), the generated tibia poses over the full motion range is obtained by rigidly transforming the tibia pose at 0° along the motion paths and refinement paths.

RESULTS: This study followed the validation procedure used in [1] to measure the accuracy of CFM. Specifically, for each ground truth pose, the generated tibia pose that corresponds to a particular ground-truth pose was identified by finding the generated pose that has smallest Hausdorff distance from the ground-truth pose. Next, the modeling error was measured in terms of 3D translation and rotation from the ground-truth pose to the corresponding generated pose. The translation and rotation were each measured as a vector with respect to the ground-truth pose based on the algorithm in [2]. Table 1 summarizes the translation and rotation errors in terms of the magnitudes of the vectors, as well as the signed-magnitudes of the vectors resolved into three principle directions, namely medial-lateral (M–L), anterior-posterior (A–P), and inferior-superior (I–S). Three symbols are used to denote each signed-magnitudes: + for significant magnitude (> 0.1 mm for translation, $> 0.1^\circ$ for rotation) in the medial, anterior, and inferior directions; – for significant magnitude in the lateral, posterior, and superior direction; and 0 for insignificant magnitude in the principle directions. Table 1 shows that the translation and rotation errors vary across different subjects and flexion angles. For translation errors, their error magnitudes range from 0.49 to 4.08 mm with no consistent direction of errors across subjects and within a subject. For rotation errors, most subjects have error magnitudes below 0.2° with no significant direction of errors. Subject S1's rotation errors at 90° and 120° flexion angles are slightly larger along the superior direction.

DISCUSSION: The magnitudes of translation and rotation errors reported in this study are larger than those reported in [1] which are 0.3 – 2.7 mm and $\leq 0.1^\circ$, respectively. One possible reason is that CFM achieves better accuracy when the modelled joint motion is mainly constrained by the bones, as for PF joint motion. When compared to the previous works that modeled and validated TF joint motion [3, 4], the reported translation errors range from 0.5 – 0.8 and 0.6 – 2.4 mm, respectively, and the reported rotation errors range from 0.5° – 6.6° and 0.9° – 3.3° , respectively. In comparison, the rotation error of our approach is significantly smaller, whereas the largest translation error is comparable for subject S2 and S3, and slightly larger for S1, S4 and S5. Moreover, the previous works requires auxiliary inputs such as bi-plane fluoroscopic video, whereas CFM requires only one set of CT scan. and Nevertheless, these amounts of errors are clinically insignificant for pre-operative planning of knee surgery. Therefore, CFM may be reliable enough to model other joints' motion while maintaining sufficient accuracy for pre-operative planning. The main limitation of this study is the small dataset size which might not capture sufficient variations across subjects. Future work may include increasing the dataset size and modeling other joints' motion that have significantly different motion characteristic as compared to TF and PF joint motion, such as shoulder and temporomandibular joints.

SIGNIFICANCE: This study highlights the potential of CFM proposed by [1] to model other joints' motion with sufficiently small errors. Thus, it strengthens the feasibility of CFM to be applied in a broader range of routine clinical practice of pre-surgical planning.

REFERENCES: [1] Hartanto, J. et al. Proc. of 2020 Annual Meeting of Orthopaedics Research Society. [2] Horn, B. et al. J. Opt. Soc. Am. A., Opt., Image, Sci., Vis. 5:1127–1135, 1988. [3] Sharma, G. B. et al. Bone Joint Res. 1(10):263-271, 2012. [4] Li, J.-S. et al. J. Biomech. Eng. 136(12):124503, 2014.

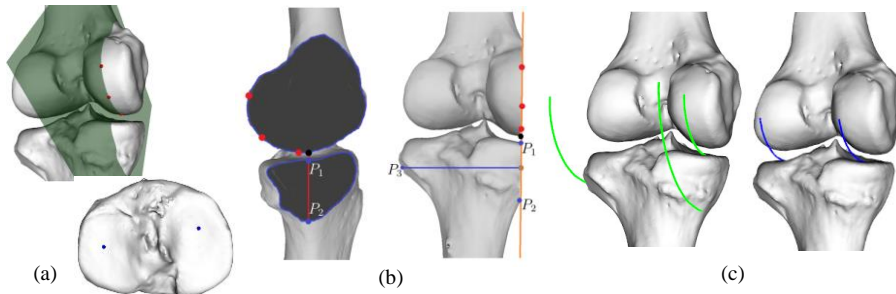


Fig.1. Three stages in contact surface model. (a) Motion plane (green plane) fits the condyle landmarks (red dots). The most proximal condyle landmark denotes the end of tibia motion. Refinement landmarks (blue) account the tilting and external/internal rotation of tibia motion. (b) Intersecting curves and distinctive points on the tibia. Intersection curves (blue) are obtained by intersecting the motion plane (green) with the tibia and femur models. Part of bone models are removed for visual clarity. Surface normal at the closest point on the femur (black dot) intersects the tibia intersecting curves at two distinctive points P1 and P2. Surface normal of motion plane (green line) at mid-point (brown dot) of the two distinctive points intersects the tibia surface at a third distinctive point P3. (c) The three motion paths (green) and two refinement paths (blue) that estimate full range of tibia motion.

Table 1. Errors of generated tibia pose at various flexion angles. Refer to main text for explanation of these symbols.

		(a) Translation errors.				(b) Rotation errors.				
		30°	60°	90°	120°	30°	60°	90°	120°	
S1		1.24	1.07	1.69	3.08		0.00	0.05	0.20	0.41
		- + -	+ 0 -	+ + -	+ + -		0.00	0.00	0.00	0.00
S2		1.25	1.78	1.97	2.27		0.00	0.00	0.00	0.00
		- - -	- 0 -	- + -	- + -		0.00	0.00	0.00	0.00
S3		0.49	0.79	2.55	4.08		0.08	0.06	0.07	0.08
		+ 0 +	+ + +	- + -	- + -		0.00	0.00	0.00	0.00
S4		1.39	2.39	3.63	3.91		0.00	0.00	0.00	0.04
		- + 0	- + -	- + -	- + -		0.00	0.00	0.00	0.00
S5		0.53	0.81	1.42	2.55		0.00	0.00	0.00	0.03
		+ 0 -	+ 0 -	- + -	- + -		0.00	0.00	0.00	0.00